Energy model of a fuel cell hybrid-electric regional train in passenger transport service and vehicle-to-grid applications

Kapetanović, Marko; Núñez, Alfredo; van Oort, Niels; Goverde, Rob M.P.

DOI
10.1016/j.jrtpm.2023.100415

Publication date
2023

Document Version
Final published version

Published in
Journal of Rail Transport Planning and Management

Journal of Rail Transport Planning & Management 28 (2023) 100415

Contents lists available at ScienceDirect

Journal of Rail Transport Planning & Management

journal homepage: www.elsevier.com/locate/jrtpm

Energy model of a fuel cell hybrid-electric regional train in passenger transport service and vehicle-to-grid applications

Marko Kapetanović [a,*], Alfredo Núñez [b], Niels van Oort [a], Rob M.P. Goverde [a]

[a] Department of Transport and Planning, Delft University of Technology, P.O. Box 5048, 2600 GA, Delft, the Netherlands
[b] Section of Railway Engineering, Delft University of Technology, P.O. Box 5048, 2600 GA, Delft, the Netherlands

ARTICLE INFO

Keywords:
Regional railways
Hydrogen
Fuel cell hybrid-electric systems
Vehicle-to-grid

ABSTRACT

Hydrogen fuel cell multiple unit vehicles are acquiring a central role in the transition process towards carbon neutral trains operation in non-electrified regional railway networks. In addition to their primary role as a transport mean, these vehicles offer significant potential for applications in innovative concepts such as smart grids. Compared to the pure electric propulsion systems, fuel cell technology allows for cogeneration processes by recovering generated heat in addition to the provision of the electrical power. This paper presents the analysis of fuel cell hybrid-electric multiple unit vehicle employed in regional railway transport during regular service, and in vehicle-to-grid application during the off-service hours, providing the electrical and thermal energy for stationary consumers in terminal stations. The system dynamics are modelled using a backward-looking quasi-static simulation approach, with implemented real-time optimization-based control strategy for managing the power flows between different components. In a case study of selected vehicle and railway services in the Netherlands, the fuel cell system showed average hydrogen consumption of 0.4 kg/km, with the overall electrical efficiency of 38.89%. In vehicle-to-grid scenario, the system satisfied complete stationary power demand, and provided about 327 kWh of thermal energy during 2-h operation, reaching the overall cogeneration efficiency of 66.81%.

1. Introduction

Increasing penetration of renewable energy sources and innovative smart grids are foreseen to have a central role in the future energy sectors globally. Electric vehicles (EVs) are recognized as one of the main elements in smart grid applications. With this concept, in addition to their primary role as a transport mean, EVs are used as a stationary energy source in vehicle-to-grid (V2G) applications (Calise et al., 2021), where they provide the power for covering grid oscillations or supplying stationary consumers such as buildings, or they use the power from the grid for re-charge (Morais et al., 2014). The global initiative of phasing-out internal combustion engines from production as of 2035 will stipulate significant increase in EV fleets worldwide, offering huge potential for their employment in smart grid applications, and at the same time raising significant challenges in the energy management of such systems. This has encouraged extensive research in the last decade, with 67 completed or on-going projects and almost 2000 papers published (Bibak and Tekiner-Moğulkoç, 2021), focussing mainly on the impacts and future challenges of V2G applications.

* Corresponding author.
E-mail addresses: M.Kapetanovic@tudelft.nl (M. Kapetanović), A.A.NunezVicencio@tudelft.nl (A. Núñez), N.vanOort@tudelft.nl (N. van Oort), R.M.P.Goverde@tudelft.nl (R.M.P. Goverde).

https://doi.org/10.1016/j.jrtpm.2023.100415
Received 31 May 2023; Received in revised form 2 August 2023; Accepted 29 September 2023
Available online 10 October 2023

Nomenclature

Abbreviations

AC	alternating current
DC	direct current
EV	electric vehicle
EMCS	energy management and control strategy
ESS	energy storage system
FCEV	fuel cell electric vehicle
FCHEMU	fuel cell hybrid-electric multiple unit
GTW	Gelenktriebwagen
HVAC	heating, ventilation and air conditioning
PEMFC	polymer electrolyte membrane (proton-exchange membrane) fuel cell
PI	partial integration
PLR	part load ratio
SQP	sequential quadratic programming
SoC	state-of-charge
V2G	vehicle-to-grid

Parameters

d_w	wheel diameter [m]
g	gravitational acceleration [m/s^2]
i_{ag}	constant gear ratio [−]
$I_{bat}^{cont,ch}$	allowed maximum continuous charging current of the battery [A]
$I_{bat}^{cont,dch}$	allowed maximum continuous discharging current of the battery [A]
$I_{bat}^{peak,ch}$	allowed peak (pulse) charging current of the battery [A]
$I_{bat}^{peak,dch}$	allowed peak (pulse) discharging current of the battery [A]
LHV_{H_2}	hydrogen low heating value [MJ /kg]
m_{fc}^{avg}	average hydrogen mass flow rate [kg /s]
m_{pax}	total weight of passengers [kg]
m_{tare}	empty vehicle mass [kg]
m_v	total vehicle mass [kg]
$P_{aux,const}$	constant auxiliaries power [W]
p_{cool}	cooling power coefficient [−]
P_{fc}^{avg}	average electric output power of the fuel cell stack [W]
P_{fc}^{rated}	rated power of the fuel cell [W]
Q_{bat}	nominal capacity of the battery [As]
R_{bat}^{ch}	battery internal resistance during charge [Ω]
R_{bat}^{dch}	battery internal resistance during discharge [Ω]
r_0	Davis equation coefficient (constant term) [N]
r_1	Davis equation coefficient (linear term) [N /(m /s)]
r_2	Davis equation coefficient (quadratic term) [$N/(m/s)^2$]
t_{peak}^{ch}	time limit for the allowed battery pulse charging current [s]
t_{peak}^{dch}	time limit for the allowed battery pulse discharging current [s]
U_{bat}^{max}	maximum battery voltage [V]
U_{bat}^{min}	minimum battery voltage [V]
v_{max}	maximum velocity [m /s]
Δt	simulation (integration) time step [s]
η_{ag}	constant efficiency of the gearbox [−]
$\eta_{bat,conv}$	constant efficiency of the battery converter [−]
η_{fc}^{avg}	average efficiency of the fuel cell stack [−]
η_{fc}^{max}	maximum efficiency of the fuel cell stack [−]
η_{fc}^{min}	minimum efficiency of the fuel cell stack [−]
η_{fc}^{opt}	optimal efficiency of the fuel cell stack [−]
$\eta_{fc,conv}$	constant efficiency of the fuel cell converter [−]
λ	rotating mass factor [−]

ξ	equivalence factor [kg /Ws]
$\sigma_{\text{bat}}^{\text{max}}$	maximum battery state-of-charge [−]
$\sigma_{\text{bat}}^{\text{min}}$	minimum battery state-of-charge [−]
$\sigma_{\text{bat}}^{\text{nom}}$	nominal battery state-of-charge [−]

Dynamic variables

a	vehicle acceleration [m /s^2]
$E_{\text{fc,conv}}$	total electric energy provided by the fuel cell system [Ws]
F_{w}	tractive/braking effort at the wheel [N]
I_{bat}	battery current [A]
$I_{\text{bat}}^{\text{max}}$	maximum battery current [A]
$I_{\text{bat}}^{\text{max,ch}}$	maximum battery charging current defined by the manufacturer [A]
$I_{\text{bat}}^{\text{max,dch}}$	maximum battery discharging current defined by the manufacturer [A]
$I_{\text{bat}}^{\text{min}}$	minimum battery current [A]
k_{bat}	penalty coefficient for battery state-of-charge deviation from nominal value [−]
k_{fc}	penalty coefficient for fuel cell efficiency deviation from optimal value [−]
M_{fc}	cumulative fuel consumption of fuel cell [kg]
m_{fc}	hydrogen mass flow rate [kg /s]
P_{aux}	total auxiliaries power [W]
$P_{\text{aux,inv}}$	electric power provided to the auxiliaries inverter [W]
P_{bat}	electric power provided from the battery [W]
$P_{\text{bat}}^{\text{max}}$	maximum (discharging) power of the battery [W]
$P_{\text{bat}}^{\text{min}}$	minimum (charging) power of the battery [W]
$P_{\text{bat,conv}}$	electric power provided from the battery converter [W]
$P_{\text{bat}}^{\text{max}}$	maximum electric power provided from the battery converter [W]
$P_{\text{bat}}^{\text{min}}$	minimum electric power provided from the battery converter [W]
P_{fc}	electric output power of the fuel cell [W]
$P_{\text{fc,conv}}$	electric power provided from the fuel cell converter [W]
$P_{\text{fc,conv}}^{\text{max}}$	maximum electric power of the fuel cell system [W]
$P_{\text{fc,conv}}^{\text{min}}$	minimum electric power of the fuel cell system [W]
P_{mot}	electric power provided to the electric motor [W]
$P_{\text{mot,inv}}$	electric power provided to the motor inverter [W]
P_{stat}	electric power demand from stationary consumers [W]
$P_{\text{stat,inv}}$	electric power provided to the stationary inverter [W]
PLR	part load ratio [−]
Q_{fc}	total thermal energy provided by the fuel cell stack [Ws]
R_{bat}	battery internal resistance [Ω]
R_{c}	curve resistances [N]
R_{g}	grade resistances [N]
r_{te}	thermal-to-electrical ratio [−]
R_{v}	vehicle resistances [N]
s	distance traveled [m]
t	time [s]
$t_{\text{cnt}}^{\text{ch}}$	battery pulse charging time counter [s]
$t_{\text{cnt}}^{\text{dch}}$	battery pulse discharging time counter [s]
T_{mot}	torque at the mechanical output of the electric motor [Nm]
T_{w}	torque at the wheel [Nm]
U_{bat}	battery terminal voltage [V]
U_{OC}	battery open circuit voltage [V]
v	vehicle velocity [m /s]
γ	angle of the slope [rad]
$\eta_{\text{aux,inv}}$	efficiency of the auxiliaries inverter [−]
$\eta_{\text{cogeneration}}$	overall cogeneration efficiency of the fuel cell system [−]
$\eta_{\text{electrical}}$	overall electrical efficiency of the fuel cell system [−]
η_{fc}	efficiency of the fuel cell stack [−]
η_{mot}	efficiency of the electric motor [−]
$\eta_{\text{mot,inv}}$	efficiency of the motor inverter [−]
$\eta_{\text{stat,inv}}$	efficiency of the stationary inverter [−]

$\eta_{thermal}$	overall thermal efficiency of the fuel cell system [−]
σ_{bat}	battery state-of-charge [−]
φ	curve radius [m]
ω_{mot}	rotational speed of the electric motor [rad /s]
ω_w	rotational speed of the wheel [rad /s]

While the main applications in the literature concern pure EVs, several studies and projects have demonstrated promising benefits linked to V2G deployment of hydrogen fuel cell electric vehicles (FCEV), with economic and energy savings being comparable (Cao, 2016) or exceeding those of pure EVs (Qian et al., 2020). The "Car as Power Plant" project at The Green Village in the Netherlands (Oldenbroek et al., 2018) demonstrated that the FCEV used in V2G application can reduce the annual grid-imported electricity to the residential building by 70% (Robledo et al., 2018). In the project presented by İnci et al. (2021), the V2G system for a FCEV with high-voltage interface to the utility-grid achieved a cost-saving of €8.78 from €67.21 for the energy purchased from the grid based on a 24 h dynamic duty cycle. Oldenbroek et al. (2017) demonstrated the potential of replacing all positive dispatchable power plants (manly gas turbine based) in Germany by 2050 using EVs and FCEVs in balancing the system power demand. The authors presented another techno-economic analysis for two technology development scenarios and two different European climates, with considered extreme peaks in balancing never exceed more than 50% of the available FCEVs V2G capacity (Oldenbroek et al., 2019).

Compared to the extensive literature on V2G applications for cars, only few studies on heavy-duty transport are found, still concerning mainly pure EVs. For instance, electric bus-to-grid applications are presented by Zhuang and Liang (2021) and Ercan et al. (2016), while Go et al. (2018) analyzed electric trains incorporated into smart grid system. As a rare example for fuel cell systems, Miller et al. (2011) presented the results for the developed shunting locomotive employed as a 65 kW mobile backup electricity power source in a military base.

Although fuel cell systems offer significant potential from recovering and utilizing generated heat, the existing research on V2G applications, both on pure EVs and FCEVs, predominantly concerns only the electrical performance and related energy, economical and or/social benefits. Cogeneration processes are considered mainly for stationary fuel cell systems, i.e., for producing the electric power and heat used for warming up the buildings or tap water (c.f., Ham et al., 2015; Najafi et al., 2015; Özgirgin et al., 2015). The only study found that analyzed cogeneration processes for a FCEV in a V2G application is presented by Fragiacomo and Piraino (2021). The authors present the model of a hybrid fuel cell tram used as a transport mean and as a power and heat source during stabling periods. The results showed the overall system efficiency of 43% in standard tram operation, and cogenerative efficiency in V2G mode exceeding 60%, while providing thermal power capable of warming up at 45 °C almost 0.2 kg/s of tap water.

Hydrogen fuel cell multiple units are identified as a potential long-term solution in decarbonizing non-electrified regional railway networks, removing the requirement of costly electrification and the range issues linked to the battery-electric vehicles (Klebsch et al., 2020). Due to the high complexity of propulsion systems for these vehicles reflected in the co-existence of multiple power sources, one

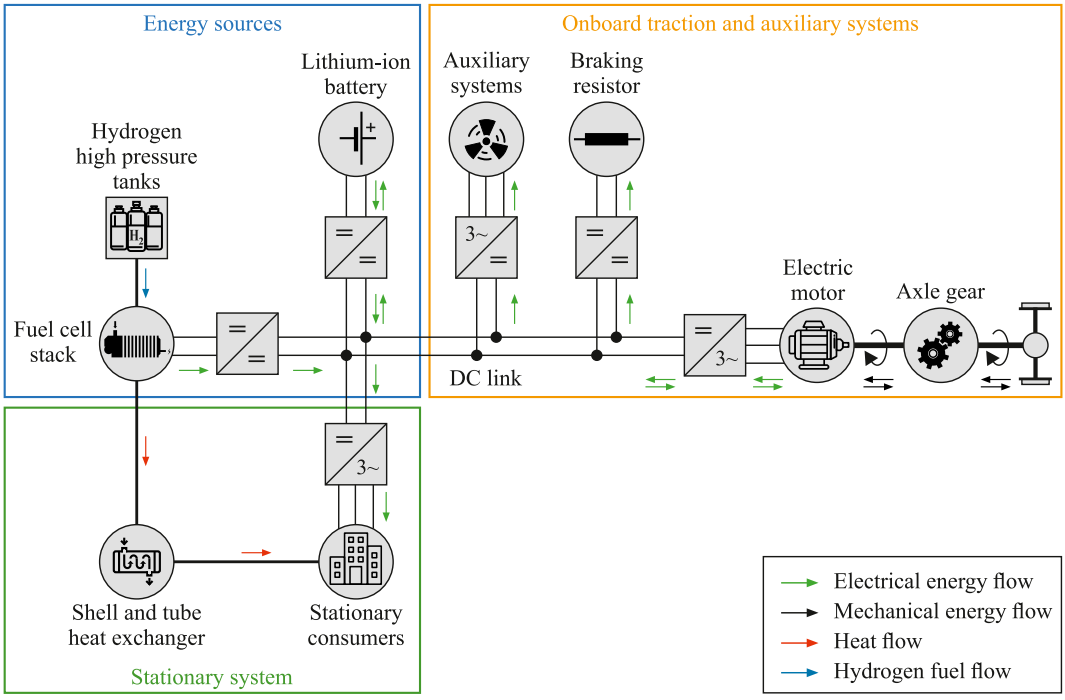

Fig. 1. Simplified schematic scheme of vehicle propulsion system and vehicle-to-grid components.

of the main challenges is the development of an energy management and control strategy (EMCS) that would ensure safe, reliable and energy-efficient system operation. Existing research contributed with a wide range of methods, with EMCSs generally classified into rule-based and optimization-based strategies (Xu et al., 2015). Rule-based strategies are based on event-triggered Boolean or fuzzy rules, designed according to powertrain characteristics or expert knowledge (Han et al., 2018; Kapetanović et al., 2021b). Due to low computation cost and storage memory, they are widely used in online (real-time) control applications, however, they typically cannot offer a proof of optimality. Dynamic programming is a proven method for solving global optimization problems (Kapetanović et al., 2021a; Tao et al., 2021), with the requirement of perfect information on future driving conditions, the long calculation time, and its nature of propagation backward in time hindering its applicability in real-time controllers. In contrast, the equivalent consumption minimization and Pontryagin's minimum principle strategies are suitable for instantaneous optimization problems (Torreglosa et al., 2011; Zhang et al., 2017). The development of causal (real-time) and implementable controls that converge to a global optimum in terms of energy use require reliable estimations of the duty cycles while satisfying requirements on the computation time and stochasticity of future conditions.

Based on the previously discussed literature, and using a regional railway network in the Netherlands as a case, this paper aims to analyze the energy performance of a fuel cell hybrid-electric multiple unit train while covering the narrow niche of V2G concept application that considers both, pure electric and cogeneration system performance. With this aim, we first provide the conceptual design of the overall system, including the main onboard and stationary components. To assess the system performance, we develop a backward-looking model equipped with the suitable optimization-based EMCS which is crucial in dispatching different power sources in the system and achieving safe and reliable operation, while at the same time minimizing the energy consumption. Lastly, we present the results of numerical experiments for a benchmark vehicle and railway services operated by Arriva.

Following Section 2 presents the description of the system with identified main components and operation principles. A detailed simulation model is provided in Section 3, with the real-time EMCS proposed in Section 4. Results for the Dutch case study are provided in Section 5. We conclude this paper with final remarks in Section 6.

2. System description

This section describes the system layout for a fuel cell hybrid-electric multiple unit (FCHEMU) vehicle employed as a transport mean in a regional railway network during the day (passenger train mode), and as electricity and heat supplier to stationary consumers during the off-service hours (V2G mode).

The entire system can be generally divided into three subsystems, as shown in Fig. 1. The energy sources are fundamental part of the system in both scenarios, providing the electrical power for onboard traction and auxiliary systems in passenger train mode, or electrical power and heat to stationary system in V2G mode. Considering non-steady duty cycles of regional passenger trains, relatively simple integration, and foreseen decrease in price of the polymer electrolyte membrane (or proton-exchange membrane) fuel cell (PEMFC) (Bagotsky et al., 2015; Sun et al., 2021), we limit the analysis in this paper to this particular fuel cell technology. Slow dynamic response of a fuel cell system requires powertrain hybridization by adding an energy storage system (ESS) that would cover rapid power oscillations and prevent fuel cell deterioration owing to starvation issues. A lithium-ion battery is considered as ESS technology, due to its commercial availability, rapid technology development and proven applications in railway sector (Ghaviha et al., 2017). The system operation in both, passenger train or V2G mode is described as follows.

2.1. Passenger train mode

In passenger train mode, fuel cell stack as the prime mover and a lithium-ion battery module as ESS provide the required power for onboard traction and auxiliary systems via a 750 V DC link. Fuel cell stack is connected to the DC link via a unidirectional DC/DC converter, which is used to adjust the stack's voltage to the DC link and prevent the damage of the fuel cell system. In this mode, the heat generated by a fuel cell system is removed by means of cooling fluid such as water-ethylene mix and onboard cooling elements, i.e., cooling radiators and fans (Fragiacomo and Piraino, 2021). A bi-directional DC/DC converter is used for the battery module to allow for both, charge and discharge phase. The mechanical power is provided to the wheels by AC motors via a constant-ratio axle gear. The motors are connected to the DC link by means of bi-directional DC/AC inverters. During braking phases, electric motors act as generators, allowing for the utilization of regenerative braking for charging the batteries, with the excess braking energy dissipated at the braking resistor. In addition to the traction motors, remaining onboard consumers include auxiliary systems such as lighting, compressors, cooling equipment, heating, ventilation and air-conditioning (HVAC) and passenger information systems. These consumers are connected to the DC link by means of unidirectional DC/AC inverters.

2.2. Vehicle-to-grid mode

In V2G mode, energy sources remain active with onboard traction and auxiliary systems switched-off. The DC link is now connected to the stationary unidirectional DC/AC inverter which adjusts the voltage (i.e., to 220 V or 480 V) and provides the alternating three-phase current to the stationary consumers. When used in V2G mode, a FCHEMU allows for utilization of cogeneration system. In addition to the electrical energy, the heat produced by the fuel cell system is now recovered and used for building heating or tap water warming up. For this aim, the cooling fluid is redirected to the shell and tube heat exchanger, where it warms up the external circuit water.

3. System modelling

The system dynamics are modelled using a backward-looking quasi-static simulation approach (Kapetanović et al., 2021a; Leska et al., 2017; Pröhl, 2017a; Pröhl and Aschemann, 2019a, 2019b). The simulation model is developed in MATLAB/Simulink using OPEUS Simulink toolbox (Pröhl, 2017b). We extend the Simulink toolbox and the model of a FCHEMU presented by Kapetanović et al. (2022) by including the fuel cell thermal characteristics and developing an optimization based EMCS applicable to both, passenger train and V2G operation mode. The simulation model structure (Fig. 2) reflects the physical system architecture from Fig. 1, with the individual blocks representing low-order models for the system components. Simulation of the two operation modes is achieved by disconnecting components not included in the respective system, i.e., stationary load and heat exchange system in passenger train mode, and traction and auxiliary load in the V2G mode.

Corresponding to the backward simulation approach, the inputs of the simulation model are the vehicle velocity, track geometry, and auxiliary systems power demand for passenger train mode, or stationary consumers power demand for V2G mode. The main output is given by a cumulative hydrogen consumption in both scenarios, together with the recovered thermal energy in V2G mode. The arrows indicate the numerical evaluation order of the model components, opposed to the direction of the physical power flow. In a physical system, converters are employed for the power flows control according to the EMCS implemented in the control unit, as described in Section 4. A braking resistor is used only for assessing the balance of power flows in the system, therefore it's detailed modelling is omitted. The remainder of this section describes the individual model components.

3.1. Traction load

Traction load represents the electrical power required by the traction motors at the DC link. According to the backward-looking approach, it is fully described by the velocity and track geometry profiles, and the power losses due to inefficiencies of the components along the traction chain, namely of the gearbox, electric motors, and motor inverters.

3.1.1. Velocity/track geometry

The energy-optimized velocity profile is pre-calculated using the bi-section algorithm (Leska et al., 2013), that considers optimal switching points between the acceleration, cruising, coasting and braking phases, while complying with the scheduled running times, track speed limitations, vehicle weight and maximum tractive/braking effort characteristics (Pröhl et al., 2021). It allows for phase-out of the driver style influence and fair comparison of the system performance between the two operation modes. The track geometry is represented with the angle of the slope and curve radius depending on the position on the track.

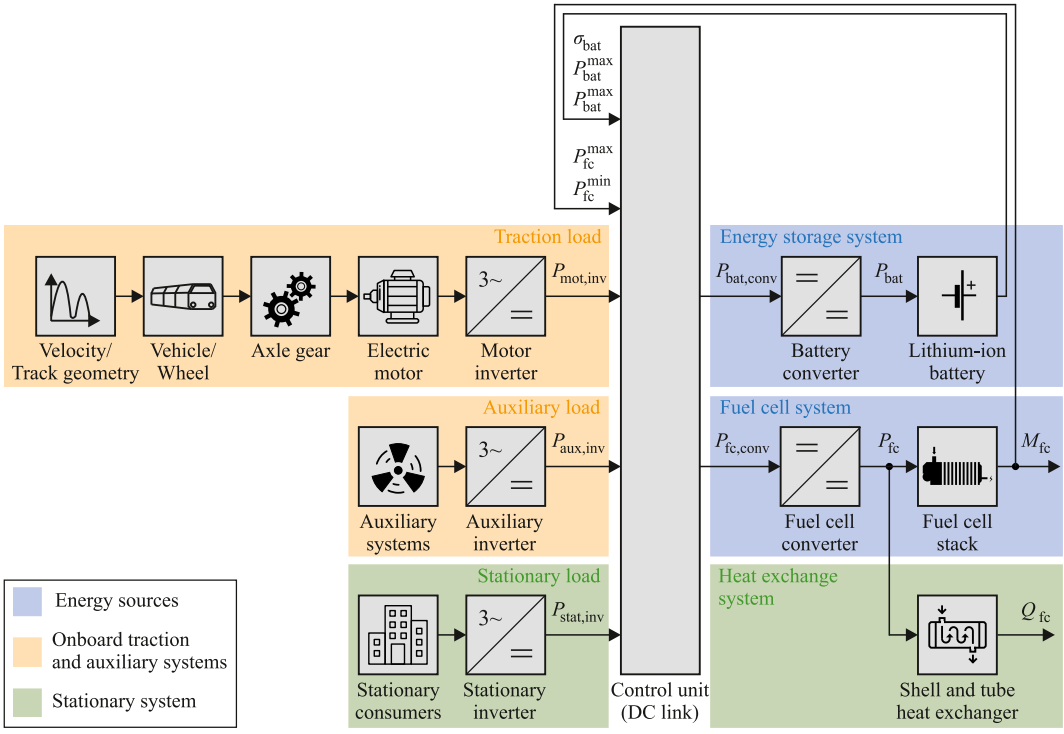

Fig. 2. Structure of the backward-looking quasi-static simulation model.

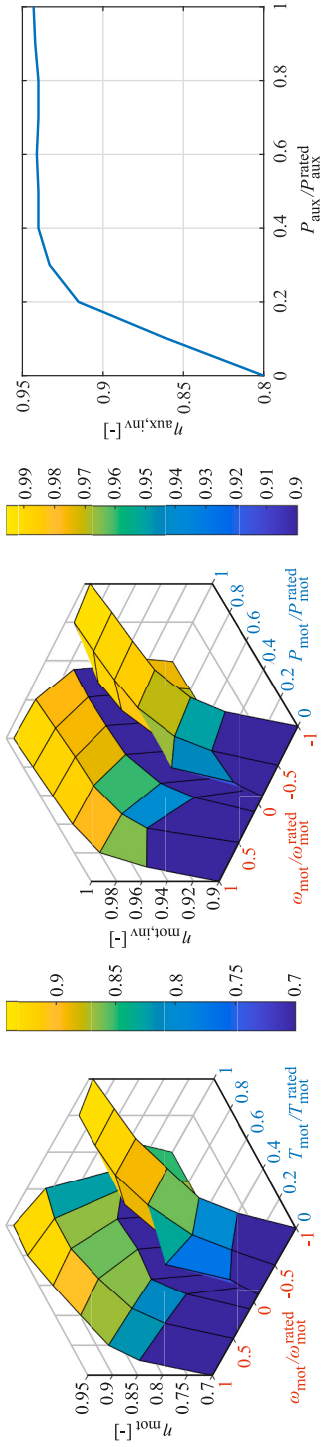

Fig. 3. Normalized efficiency map for (a) electric motor, (b) motor inverter, and (c) auxiliaries' inverter.

3.1.2. Vehicle/wheel

With the given velocity and track geometry profiles as input signals, the tractive or braking effort at the wheel F_w [N] can be expressed as

$$F_w(v(t)) = m_v \cdot a(t) + R_v(v(t)) + R_g(\gamma(s(t))) + R_c(\varphi(s(t))) \tag{1}$$

where t [s] is the time; v [m/s] is the vehicle velocity; $s = \int_0^t v(\tau)d\tau$ [m] is the distance traveled; $a = dv/dt$ [m/s^2] is the acceleration; m_v [kg] is the total mass of the vehicle which takes into account the rotary inertia of the powertrain and the passengers weight, i.e. $m_v = (1+\lambda) \cdot m_{tare} + m_{pax}$, with λ denoting the dimensionless rotating mass factor, m_{tare} [kg] the vehicle tare weight, and m_{pax} [kg] the total weight of passengers; the vehicle resistances R_v [N] include roll resistance and air resistance, modelled as a quadratic function of the vehicle velocity using the Davis equation (Davis, 1926); R_g [N] is the grade resistance calculated as a function of the angle of the slope γ [rad] (Brünger and Dahlhaus, 2014); curve resistance R_c [N] is calculated using Roeckl's formula (Huerlimann and Nash, 2003), with φ [m] denoting the curve radius. Depending on the wheel diameter d_w [m] and the train speed v, the torque at the wheel T_w [Nm] and the rotational speed of the wheel ω_w [rad/s] can be calculated as (Pröhl, 2017b):

$$T_w(t) = F_w(v(t)) \cdot \frac{d_w}{2}; \quad \omega_w(t) = 2 \cdot \frac{v(t)}{d_w}. \tag{2}$$

3.1.3. Axle gear

The axle gear transmits the mechanical power from the motors' shaft to the wheels. With the constant gear ratio i_{ag} and the constant efficiency of the gearbox η_{ag} the torque T_{mot} [Nm] and the rotational speed ω_{mot} [rad/s] at the mechanical input of the axle gear can be computed by Pröhl (2017b):

$$T_{mot}(t) = \begin{cases} \dfrac{T_w(t)}{i_{ag} \cdot \eta_{ag}} & \text{if } T_w(t) \geq 0 \\ \dfrac{T_w(t) \cdot \eta_{ag}}{i_{ag}} & \text{if } T_w(t) < 0; \end{cases} \qquad \omega_{mot}(t) = \omega_w(t) \cdot i_{ag} \tag{3}$$

3.1.4. Electric motor

Depending on the direction of the power flow (motor or generator operation mode), and with the motor's efficiency $\eta_{mot} = f_{mot}(T_{mot}, \omega_{mot})$ determined by a linear 2D-interpolation in the normalized efficiency map (Fig. 3a) provided by Pröhl (2017b), the electric power of the electric motor P_{mot} [W] can be computed by

$$P_{mot}(t) = \begin{cases} \dfrac{T_{mot}(t) \cdot \omega_{mot}(t)}{\eta_{mot}(T_{mot}(t), \omega_{mot}(t))} & \text{if } T_{mot}(t) \geq 0 \\ T_{mot}(t) \cdot \omega_{mot}(t) \cdot \eta_{mot}(T_{mot}(t), \omega_{mot}(t)) & \text{if } T_{mot}(t) < 0. \end{cases} \tag{4}$$

3.1.5. Motor inverter

The traction load at the DC link representing the electric power provided to the motor inverters $P_{mot,inv}$ [W] results from

$$P_{mot,inv}(t) = \begin{cases} \dfrac{P_{mot}(t)}{\eta_{mot,inv}(P_{mot}(t), \omega_{mot}(t))} & \text{if } P_{mot}(t) \geq 0 \\ P_{mot}(t) \cdot \eta_{mot,inv}(P_{mot}(t), \omega_{mot}(t)) & \text{if } P_{mot}(t) < 0, \end{cases} \tag{5}$$

with the efficiency of the motor inverters $\eta_{mot,inv} = f_{mot,inv}(P_{mot}, \omega_{mot})$ determined by a linear interpolation in the normalized efficiency map (Fig. 3b) given by Pröhl (2017b).

3.2. Auxiliary load

Auxiliary load represents the electrical power required by the onboard auxiliary consumers at the DC link, computed as follows.

3.2.1. Auxiliary systems

The total auxiliaries power P_{aux} [W] is modelled as the sum of the constant term $P_{aux,const}$ [W], representing constant consumers such as light and HVAC system, and the variable term which accounts for the cooling power (Pröhl and Aschemann, 2019a), i.e.

$$P_{aux}(t) = P_{aux,const} + p_{cool} \cdot |P_{mot,inv}(t)|, \tag{6}$$

where coefficient p_{cool} represents the proportion of the total traction power required for cooling the main traction components.

3.2.2. Auxiliary inverter

The resulting auxiliary load at the DC link $P_{\text{aux,inv}}$ [W] follows from

$$P_{\text{aux,inv}}(t) = \frac{P_{\text{aux}}(t)}{\eta_{\text{aux,inv}}(P_{\text{aux}}(t))}, \tag{7}$$

with the efficiency of the auxiliary inverters $\eta_{\text{aux,inv}} = f_{\text{aux,inv}}(P_{\text{aux}})$ computed by a linear interpolation in the normalized efficiency map (Fig. 3c) provided by Pröhl (2017b).

3.3. Stationary load

Stationary load is given as the electrical power demand at the DC link from stationary consumers such as appliances in the terminal station or buildings, described as follows.

3.3.1. Stationary consumers

Compared to the fast power oscillations characterizing passenger train operation, power demand of stationary consumers is usually featured with more steady duty cycles, especially during the considered off-service hours when the terminal station facilities work at low capacity (Fragiacomo and Piraino, 2021). Nevertheless, the energy sources in the hybrid power system should be able to cover deep demand fluctuations due to unexpected events. The electrical power demand from stationary consumers, P_{stat} [W], is considered as the main simulation input in V2G operation mode.

3.3.2. Stationary inverter

The total provided electrical power at the DC link, $P_{\text{stat,inv}}$ [W], accounts for the losses due to inefficiency of the DC/AC stationary inverter, with assumed normalized efficiency function $\eta_{\text{stat,inv}} = f_{\text{stat,inv}}(P_{\text{stat}})$ identical to that of the onboard auxiliary inverter (Fig. 3c), i.e.

$$P_{\text{stat,inv}}(t) = \frac{P_{\text{stat}}(t)}{\eta_{\text{stat,inv}}(P_{\text{stat}}(t))}. \tag{8}$$

3.4. Energy storage system

Energy storage system supports the fuel cell system during the high power demand, compensates for the slow dynamics of a fuel cell, and stores the regenerative braking energy, with corresponding sub-models defined as follows.

3.4.1. Battery converter

Compared to the DC/AC inverters, DC/DC converters are featured with high efficiency, ranging between 95 and 99% (Pröhl, 2017b). Therefore, to reduce the complexity of the ESS model and the EMCS, we assume a constant high efficiency of a battery converter, i.e., $\eta_{\text{bat,conv}} = 0.97$. Depending on the required power from the ESS at the DC link, $P_{\text{bat,conv}}[W]$, the power delivered from the battery, P_{bat} [W], results from

$$P_{\text{bat}}(t) = \begin{cases} \dfrac{P_{\text{bat,conv}}(t)}{\eta_{\text{bat,conv}}} & \text{if } P_{\text{bat,conv}}(t) \geq 0 \\ P_{\text{bat,conv}}(t) \cdot \eta_{\text{bat,conv}} & \text{if } P_{\text{bat,conv}}(t) < 0. \end{cases} \tag{9}$$

3.4.2. Lithium-ion battery

The simulation model of a lithium-ion battery adopted from Kapetanović et al. (2022) is implemented for the equivalent electrical

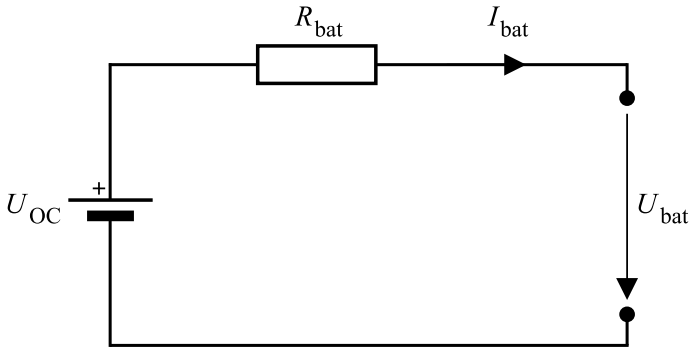

Fig. 4. Equivalent electrical circuit for a lithium-ion battery.

circuit shown in Fig. 4. The circuit consists of an open circuit voltage source U_{OC} [V], which depends on the battery state-of-charge (SoC), σ_{bat} [−], in series with a constant internal resistance R_{bat} [Ω], which represents ohmic losses and depends on the direction of the current I_{bat} [A] (i.e., whether the battery is being charged or discharged). With the given power provided from the battery, the battery current and terminal voltage U_{bat} [V] result from

$$I_{\mathrm{bat}}(t) = \frac{U_{\mathrm{OC}}(\sigma_{\mathrm{bat}}(t)) - \sqrt{U_{\mathrm{OC}}(\sigma_{\mathrm{bat}}(t))^2 - 4 \cdot P_{\mathrm{bat}}(t) \cdot R_{\mathrm{bat}}(I_{\mathrm{bat}}(t))}}{2 \cdot R_{\mathrm{bat}}(I_{\mathrm{bat}}(t))} \tag{10}$$

$$U_{\mathrm{bat}}(t) = U_{\mathrm{bat}}(\sigma_{\mathrm{bat}}(t)) - R_{\mathrm{bat}}(I_{\mathrm{bat}}(t)) \cdot I_{\mathrm{bat}}(t). \tag{11}$$

With the initial SoC $\sigma_{\mathrm{bat}}(0)$, and nominal battery capacity Q_{bat} [As], the battery SoC at time instant t results from

$$\sigma_{\mathrm{bat}}(t) = \sigma_{\mathrm{bat}}(0) - \frac{1}{Q_{\mathrm{bat}}} \cdot \int_0^t I_{\mathrm{bat}}(\tau) d\tau. \tag{12}$$

The maximum (discharging) power $P_{\mathrm{bat}}^{\mathrm{max}}$ [W] and minimum (charging) power $P_{\mathrm{bat}}^{\mathrm{min}}$ [W] are limited by the maximum and minimum current, $I_{\mathrm{bat}}^{\mathrm{max}}$ [A] and $I_{\mathrm{bat}}^{\mathrm{min}}$ [A], while keeping the limits of the SoC $[\sigma_{\mathrm{bat}}^{\mathrm{min}}, \sigma_{\mathrm{bat}}^{\mathrm{max}}]$, battery voltage $[U_{\mathrm{bat}}^{\mathrm{min}}, U_{\mathrm{bat}}^{\mathrm{max}}]$, and allowed short peak values:

$$P_{\mathrm{bat}}^{\mathrm{max}}(t) = \left(U_{\mathrm{OC}}(\sigma_{\mathrm{bat}}(t)) - R_{\mathrm{bat}}^{\mathrm{dch}} \cdot I_{\mathrm{bat}}^{\mathrm{max}}(t)\right) \cdot I_{\mathrm{bat}}^{\mathrm{max}}(t) \tag{13}$$

$$P_{\mathrm{bat}}^{\mathrm{min}}(t) = \left(U_{\mathrm{OC}}(\sigma_{\mathrm{bat}}(t)) - R_{\mathrm{bat}}^{\mathrm{ch}} \cdot I_{\mathrm{bat}}^{\mathrm{min}}(t)\right) \cdot I_{\mathrm{bat}}^{\mathrm{min}}(t) \tag{14}$$

with

$$I_{\mathrm{bat}}^{\mathrm{max}}(t) = \min\left\{\frac{U_{\mathrm{OC}}(\sigma_{\mathrm{bat}}(t)) - U_{\mathrm{bat}}^{\mathrm{min}}}{R_{\mathrm{bat}}^{\mathrm{dch}}}, \frac{(\sigma_{\mathrm{bat}}(t) - \sigma_{\mathrm{bat}}^{\mathrm{min}}) \cdot Q_{\mathrm{bat}}}{\Delta t}, I_{\mathrm{bat}}^{\mathrm{max,dch}}(t)\right\} \tag{15}$$

$$I_{\mathrm{bat}}^{\mathrm{min}}(t) = \max\left\{\frac{U_{\mathrm{OC}}(\sigma_{\mathrm{bat}}(t)) - U_{\mathrm{bat}}^{\mathrm{max}}}{R_{\mathrm{bat}}^{\mathrm{ch}}}, \frac{(\sigma_{\mathrm{bat}}(t) - \sigma_{\mathrm{bat}}^{\mathrm{max}}) \cdot Q_{\mathrm{bat}}}{\Delta t}, I_{\mathrm{bat}}^{\mathrm{max,ch}}(t)\right\} \tag{16}$$

where Δt [s] is the integration time step, and $I_{\mathrm{bat}}^{\mathrm{max,dch}}$ and $I_{\mathrm{bat}}^{\mathrm{max,ch}}$ are the maximum discharging and charging current, defined by the maximum permitted continuous values ($I_{\mathrm{bat}}^{\mathrm{cont,dch}}$, $I_{\mathrm{bat}}^{\mathrm{cont,ch}}$) or the pulse values ($I_{\mathrm{bat}}^{\mathrm{peak,dch}}$, $I_{\mathrm{bat}}^{\mathrm{peak,ch}}$) allowed for the limited time ($t_{\mathrm{peak}}^{\mathrm{dch}}$; $t_{\mathrm{peak}}^{\mathrm{ch}}$) and controlled by the corresponding time counters ($t_{\mathrm{cnt}}^{\mathrm{dch}}$; $t_{\mathrm{cnt}}^{\mathrm{ch}}$), i.e.

$$I_{\mathrm{bat}}^{\mathrm{max,dch}}(t) = \begin{cases} I_{\mathrm{bat}}^{\mathrm{peak,dch}} & \text{if } t_{\mathrm{cnt}}^{\mathrm{dch}}(t) < t_{\mathrm{peak}}^{\mathrm{dch}} \\ I_{\mathrm{bat}}^{\mathrm{cont,dch}} & \text{if } t_{\mathrm{cnt}}^{\mathrm{dch}}(t) \geq t_{\mathrm{peak}}^{\mathrm{dch}} \end{cases} \tag{17}$$

$$I_{\mathrm{bat}}^{\mathrm{max,ch}}(t) = \begin{cases} I_{\mathrm{bat}}^{\mathrm{peak,ch}} & \text{if } t_{\mathrm{cnt}}^{\mathrm{ch}}(t) < t_{\mathrm{peak}}^{\mathrm{ch}} \\ I_{\mathrm{bat}}^{\mathrm{cont,ch}} & \text{if } t_{\mathrm{cnt}}^{\mathrm{ch}}(t) \geq t_{\mathrm{peak}}^{\mathrm{ch}}. \end{cases} \tag{18}$$

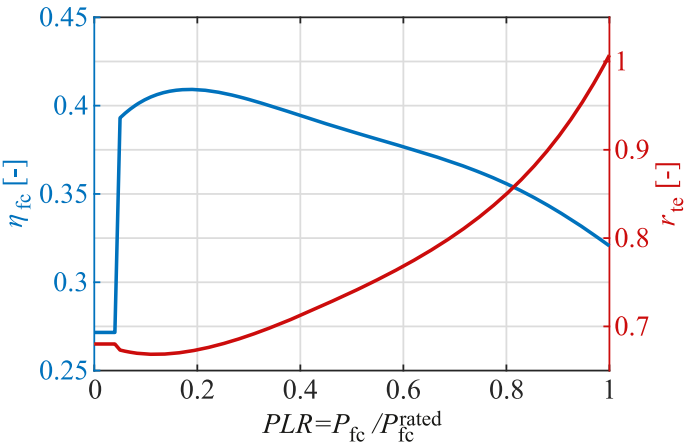

Fig. 5. Normalized efficiency and thermal-to-electrical ratio functions of a fuel cell.

3.5. Fuel cell system

Modelling of a fuel cell system, consisted of a PEMFC stack and unidirectional DC/DC converter is described as follows.

3.5.1. Fuel cell converter

We assume high constant efficiency of a fuel cell DC/DC converter, identical to the one of the ESS, i.e., $\eta_{\text{fc,conv}} = 0.97$. With the requested power from the fuel cell system at the DC link, $P_{\text{fc,conv}}$ [W], and according to the backward-looking approach, the output power of a fuel cell stack P_{fc} [W] results from

$$P_{\text{fc}}(t) = \frac{P_{\text{fc,conv}}(t)}{\eta_{\text{fc,conv}}}. \tag{19}$$

3.5.2. Fuel cell stack

Implemented PEMFC model aims to assess hydrogen consumption and recovered thermal energy, while including the dynamics and efficiency of a fuel cell system. The electrical efficiency $\eta_{\text{fc}} = f_{\text{fc}}(PLR(t))$ and thermal-to-electrical ratio $r_{\text{te}} = f_{\text{te}}(PLR(t))$ of a fuel cell system are determined using an approximated function of the normalized fuel cell electrical output power by its rated power $P_{\text{fc}}^{\text{rated}}$ [W], referred as part load ratio (PLR), i.e., $PLR = P_{\text{fc}}/P_{\text{fc}}^{\text{rated}}$ (Maleki and Rosen, 2017), as given in the following equations and Fig. 5:

$$\eta_{\text{fc}}(PLR(t)) = \begin{cases} 0.2716, & \text{if } (PLR) < 0.05 \\ 0.9033 \cdot (PLR(t))^5 - 2.9996 \cdot (PLR(t))^4 & \\ +3.6503 \cdot (PLR(t))^3 - 2.0704 \cdot (PLR(t))^2 & \text{if } (PLR) \geq 0.05. \\ +0.4623 \cdot (PLR(t)) + 0.3747 & \end{cases} \tag{20}$$

$$r_{\text{te}}(PLR(t)) = \begin{cases} 0.6801, & \text{if } (PLR) < 0.05 \\ 1.0785 \cdot (PLR(t))^4 - 1.9739 \cdot (PLR(t))^3 & \\ +1.5005 \cdot (PLR(t))^2 - 0.2817 \cdot (PLR(t)) & \text{if } (PLR) \geq 0.05. \\ +0.6838 & \end{cases} \tag{21}$$

With the requested electrical power from the fuel cell, $P_{\text{fc}}(t)$, cumulative hydrogen consumption M_{fc} [g] at time instant t is calculated by:

$$M_{\text{fc}}(t) = \int_0^t m_{\text{fc}}(\tau)d\tau = \int_0^t \frac{P_{\text{fc}}(\tau)}{LHV_{\text{H}_2} \cdot \eta_{\text{fc}}(PLR(\tau))} d\tau, \tag{22}$$

where m_{fc} [g] is the hydrogen mass flow rate, and LHV_{H_2} is the hydrogen low heating value (120 MJ/kg) (Sarma and Ganguly, 2018).

In addition, we model the slow dynamic response of the PEMFC auxiliary components which imposes the limitation on the rate of change of PEMFC output power P_{fc} (Barbir, 2013). Based on the premise that the PEMFC requires 30 s from a start-up to reaching 90% of its rated power (Pesaran et al., 2005), the limitation of the rate of change of its output power is defined by the following constraint

$$\left| \frac{dP_{\text{fc}}}{dt} \right| \leq 0.03 \cdot P_{\text{fc}}^{\text{rated}} \left[\frac{\text{W}}{\text{s}} \right]. \tag{23}$$

The overall electrical efficiency $\eta_{\text{electrical}}$ is determined by considering the losses due to inefficiencies of the fuel cell converter and fuel cell stack, where $E_{\text{fc,conv}}(T) = \int_0^T P_{\text{fc,conv}}(\tau)d\tau$ [Ws] represents the total electrical energy provided at the DC link, and T [s] is the total duration of the system operation:

$$\eta_{\text{electrical}} = \frac{E_{\text{fc,conv}}(T)}{M_{\text{fc}}(T) \cdot LHV_{\text{H}_2}}. \tag{24}$$

3.6. Shell and tube heat exchanger

The total thermal energy received by the heat exchanger from the fuel cell system Q_{fc} [Ws] at time instant t is calculated by:

$$Q_{\text{fc}}(t) = \int_0^t P_{\text{fc}}(\tau) \cdot r_{\text{te}}(PLR(\tau))d\tau. \tag{25}$$

The overall thermal efficiency in V2G mode, η_{thermal}, is calculated as the ratio of the total thermal energy provided and the hydrogen energy in input, as given in (26). Finally, the cogeneration efficiency, $\eta_{\text{cogeneration}}$, is achieved as the sum of the electrical and thermal one, as shown in (27),

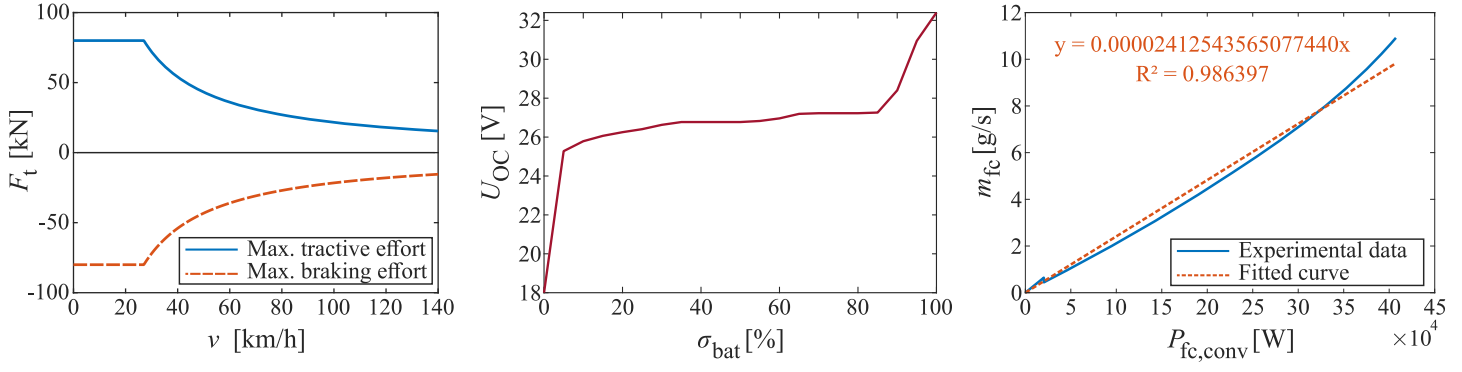

Fig. 6. (a) Vehicle maximum tractive and braking effort; (b) open circuit voltage function for a lithium-ion battery module; (c) relationship between hydrogen consumption rate and power delivered by the fuel cell system.

$$\eta_{\text{thermal}} = \frac{Q_{\text{fc}}(T)}{M_{\text{fc}}(T) \cdot LHV_{\text{H}_2}} \tag{26}$$

$$\eta_{\text{cogeneration}} = \eta_{\text{electrical}} + \eta_{\text{thermal}} \tag{27}$$

4. Energy management and control strategy

The aim of the EMCS implemented in the control unit is to distribute total demanded power for traction and auxiliaries between different power sources in the system, while minimizing total hydrogen consumption. A real-time and implementable control based on equivalent consumption minimization strategy is defined in this study. The concept of equivalent fuel consumption was introduced by Paganelli et al. (2002) with the aim to define instantaneous optimization EMCS. It is based on transforming the electrical energy consumption of the ESS into equivalent fuel consumption, making different energy forms (i.e. fuel and electrical) from different energy sources in the hybrid system comparable.

EMCS proposed in this paper is based on minimizing the sum of instantaneous equivalent hydrogen consumption from the battery system and direct hydrogen consumption from the fuel cell system, while satisfying the constraints that allow for normal operation of different power sources. The optimization problem is formulated as

$$\min_{\{P_{\text{fc,conv}}, P_{\text{bat,conv}}\}} \left(k_{\text{fc}} \cdot m_{\text{fc}}\left(P_{\text{fc,conv}}(t)\right) + k_{\text{bat}} \cdot \xi \cdot P_{\text{bat,conv}}(t)\right) \tag{28}$$

subject to

$$P_{\text{fc,conv}}(t) + P_{\text{bat,conv}}(t) = \begin{cases} P_{\text{mot,inv}}(t) + P_{\text{aux,inv}}(t) & \text{for passenger train mode} \\ P_{\text{stat,inv}}(t) & \text{for V2G mode} \end{cases} \tag{29}$$

$$P^{\min}_{\text{fc,conv}}(t) \le P_{\text{fc,conv}}(t) \le P^{\max}_{\text{fc,conv}}(t) \tag{30}$$

$$P^{\min}_{\text{bat,conv}}(t) \le P_{\text{bat,conv}}(t) \le P^{\max}_{\text{bat,conv}}(t) \tag{31}$$

where k_{fc} and k_{bat} are the penalty coefficients accounting for fuel cell efficiency and battery SoC deviation from the optimal/nominal values, m_{fc} is the fuel cell instantaneous hydrogen consumption calculated by (19), (20) and (22), and ξ is the equivalence factor, defined by

$$\xi = \frac{m^{\text{avg}}_{\text{fc}}}{P^{\text{avg}}_{\text{fc}} \cdot \eta_{\text{fc,conv}}} = \frac{1}{LHV_{\text{H}_2} \cdot \eta^{\text{avg}}_{\text{fc}} \cdot \eta_{\text{fc,conv}}}, \tag{32}$$

with $m^{\text{avg}}_{\text{fc}}$, $P^{\text{avg}}_{\text{fc}}$ and $\eta^{\text{avg}}_{\text{fc}}$ denoting the average hydrogen consumption rate, power and efficiency of a fuel cell stack, respectively. Since the future power demand is unknown, we determine the equivalent hydrogen consumption of the ESS from the relationship $m^{\text{avg}}_{\text{fc}} / \left(P^{\text{avg}}_{\text{fc}} \cdot \eta_{\text{fc,conv}}\right)$ in (32) as a fitted curve slope factor for considered fuel cell system (Fig. 6c). The constraint (29) ensures that the total instantaneous power demand in both, passenger train or V2G mode, is satisfied from the two power sources. In (30), the lower and upper limit of the instantaneous power from the fuel cell system, $P^{\min}_{\text{fc,conv}}$ and $P^{\max}_{\text{fc,conv}}$, respectively, are determined from (19) and (23), and according to the overall power range $P_{\text{fc,conv}} \in \left[0, P^{\text{rated}}_{\text{fc}} \cdot \eta_{\text{fc,conv}}\right]$. Similarly, in (31), the limits of the instantaneous power from the ESS, $P^{\min}_{\text{bat,conv}}$ and $P^{\max}_{\text{bat,conv}}$, are computed using (9) and (13)–(18). Note that the limits of the battery SoC are already represented in the battery model via power limitations, thus, separate constraint on the battery SoC is not imposed in the present optimization problem.

Different approaches in solving given optimization problem have been proposed. For instance, Zhang et al. (2017) used linear penalty functions and second order polynomial approximations of hydrogen consumption to derive analytical solution to the problem defined in (28). The obtained power distribution is subsequently adjusted using partial integration (PI) controllers in order to satisfy the constraints, leading to its deviation from the optimal one. In this paper, EMCS is transformed into a nonlinear constrained optimization problem (Li et al., 2019), allowing for direct implementation of the optimal solution. The penalty coefficients in (28) are given by

$$k_{\text{fc}} = \left(1 - \frac{2 \cdot \left(\eta_{\text{fc}}(t) - \eta^{\text{opt}}_{\text{fc}}\right)}{\eta^{\max}_{\text{fc}} - \eta^{\min}_{\text{fc}}}\right)^2 \tag{33}$$

$$k_{\text{bat}} = \left(1 - \frac{2 \cdot \left(\sigma_{\text{bat}}(t) - \sigma^{\text{nom}}_{\text{bat}}\right)}{\sigma^{\max}_{\text{bat}} - \sigma^{\min}_{\text{bat}}}\right)^4, \tag{34}$$

where $\eta^{\text{opt}}_{\text{fc}}$, $\eta^{\max}_{\text{fc}}$ and $\eta^{\min}_{\text{fc}}$ are the optimal, maximum and minimum efficiency of the fuel cell stack, determined from (20), and $\sigma^{\text{nom}}_{\text{bat}}$ is the nominal battery SoC, i.e., $\sigma^{\text{nom}}_{\text{bat}} = \sigma_{\text{bat}}(0)$.

We use the sequential quadratic programming (SQP) approach to solve this nonlinear constrained problem. The SQP method generates steps by solving quadratic subproblems and it can be used both in line search and trust-region frameworks (Fletcher, 2010). We implement the *fmincon* function in the Simulink model to minimize the hydrogen consumption and find the optimal power distribution between the fuel cell system and the battery at each time instant, according to (28)–(34).

5. Case study of the Dutch regional trains in the Northern lines

This section presents a case study of selected multiple unit vehicle and services operated by Arriva in the Northern lines in the Netherlands. Stadler's two-coach multiple unit vehicle from the series GTW, currently utilized in the Northern lines (Stadler, 2005), is selected as the benchmark vehicle. We adopt the fuel cell hybrid-electric system design for this particular vehicle from Kapetanović et al. (2022). The required input parameters are provided in Table 1. The maximum tractive/braking effort used for generating the speed profile is shown in Fig. 6a, and SoC function for a battery module in Fig. 6b.

5.1. Passenger train operation

The system performance in passenger train mode is evaluated for the railway service provided by Arriva between stations Leeuwarden and Groningen, with the track and timetable input parameters adopted from Kapetanović et al. (2022), and given in Fig. 7.

The simulation output for the operation of selected benchmark vehicle performing a round trip between stations Leeuwarden and Groningen is provided in Fig. 8. Using pre-generated energy-optimized velocity profile (Fig. 8a) as the main simulation input, the total power required by traction and auxiliary systems at the DC link is evaluated and distributed between the two power sources, i.e., the fuel cell and energy storage systems, by employing the equivalent consumption minimization strategy (Fig. 8b). The proposed EMCS ensured proper operation of the system components, while providing the sustenance of the battery SoC (Fig. 8c) and operation of the

Table 1
Vehicle and propulsion system parameters for Stadler GTW FCHEMU.

Parameter	Value	Unit
General vehicle parameters		
Tare weight[a)]	71.787	t
Rotating mass factor[b)]	0.05	–
Total passengers weight[b)]	7	t
Davis equation coefficient (constant term)[c)]	1001	N
Davis equation coefficient (linear term)[c)]	22.3	N/(km/h)
Davis equation coefficient (quadratic term)[c)]	0.1	$N/(km/h)^2$
Powered wheel diameter[d)]	0.86	m
Axle gear ratio[e)]	1.7218	–
Axle gear efficiency[b)]	0.97	–
Maximum velocity[d)]	140	km/h
Maximum acceleration[c)]	1.05	m/s^2
Maximum deceleration[b)]	−1	m/s^2
Electric motors rated power[f)]	2 × 400	kW
Constant auxiliaries power[b)]	50	kW
Cooling power coefficient[b)]	0.01	–
Fuel cell system		
Rated power[g)]	70	kW
Idle power[g)]	8	kW
Number of modules[a)]	6	–
Hydrogen storage system		
Hydrogen capacity per cylinder[h)]	7.8	kg
Number of cylinders[a)]	23	–
Energy storage system[c)]		
Nominal capacity[i)]	45	Ah
Minimum/maximum continuous current[i)]	−160/160	A
Minimum/maximum pulse current[i)]	−350/350	A
Allowed time for pulse current[i)]	10	s
Minimum/maximum voltage[i)]	18/32.4	V
Internal resistance charge/discharge[i)]	0.006/0.006	Ω
Nominal SoC[b)]	50	%
Minimum/maximum SoC[b)]	10/90	%
Energy content[i)]	1.24	kWh
Useable energy content[j)]	0.922	kWh
Number of modules[a)]	157	–

Source/Note: [a)] Kapetanović et al. (2022); [b)] Assumed/adopted values for simulation purposes; [c)] Provided by Arriva; [d)] Stadler (2005); [e)] Determined from the ratio between the maximum rotational speed of the GTW's motor provided by Giro Batalla and Feenstra (2012) and the maximum rotational speed of the wheel corresponding to the maximum vehicle speed; [f)] Giro Batalla and Feenstra (2012); [g)] Ballard (2023); [h)] Luxfer (2023); [i)] Toshiba (2023); [j)] Based on allowed SoC range.

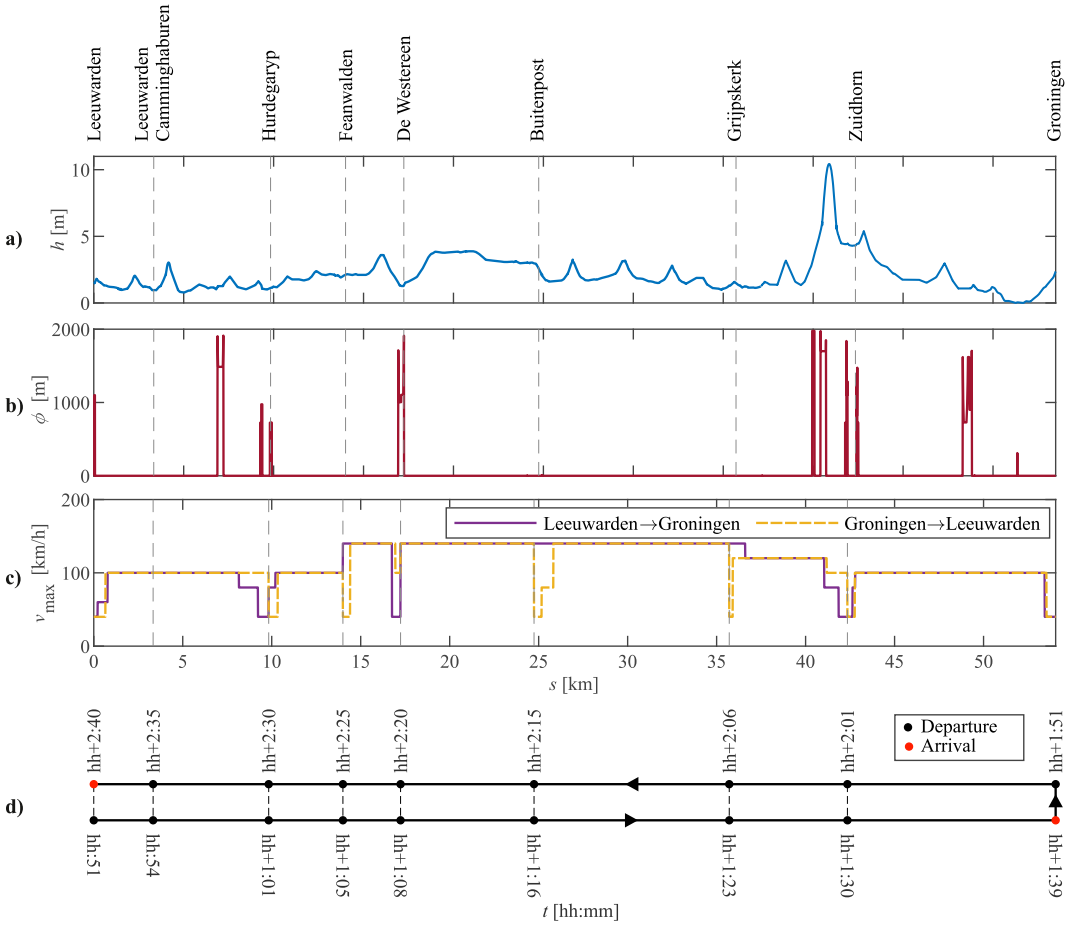

Fig. 7. Railway line Leeuwarden – Groningen: (a) track height compared to Normal Amsterdam Level; (b) position and dimeter of track curves; (c) maximum allowed speed; and (d) train departure times for the two opposite directions.

fuel cell system in a high-efficiency region (above 40%) for most of the trip duration (Fig. 8d). The estimated hydrogen consumption for the 2-h duty cycle is 22.019 kg, with approximately 0.4 kg/km, which is in line with the conventional railway vehicles. The fuel cell system provided in total 284.907 kWh electrical energy at the DC link, resulting with the overall electrical efficiency of 38.82%.

5.2. *Vehicle-to-grid operation*

The system performance in a V2G mode is assessed for a hypothetical power demand from the stationary consumers in Leeuwarden terminal station during a 2-h operation interval. Although stationary consumers are typically featured with steady power demand, especially during off-service hours, to assess the system performance under different load conditions, the requested electrical power $P_{\text{stat}}(t)$ is represented with a step-wise power profile, consisted of constant-power phases randomly generated within the power interval $[0\ \text{kW}, 420\ \text{kW}]$ with corresponding duration randomly selected within the time interval $[5\ \text{min}, 15\ \text{min}]$.

The generated power profile at the DC link for stationary electrical consumers, and the power distribution between the fuel cell and energy storage systems are given in Fig. 9a, with the resulting battery SoC shown in Fig. 9b. The EMCS ensured functioning of the power sources within permitted limits, while balancing the requirement of battery SoC sustenance and high-efficiency fuel cell operation. The total calculation time for a 2-h duty cycle was about 2.5 min for both, passenger train and V2G scenarios, confirming the real-time application potential of the proposed EMCS.

Due to the imposed sudden power jumps followed by a high constant power demand, fuel cell stack mostly operated in lower efficiency regions compared to the standard passenger train duty cycle (Fig. 9c). The estimated hydrogen consumption in this case was 33.797 kg, with provided 425.583 kWh of electrical energy, resulting with the overall electrical efficiency of 37.78%. At the same time, the fuel cell stack provided 327.074 kWh of thermal energy to the shell and tube heat exchanger, with the overall thermal efficiency of 29.03%. Thus, the total cogeneration efficiency of 66.81% was reached in V2G mode.

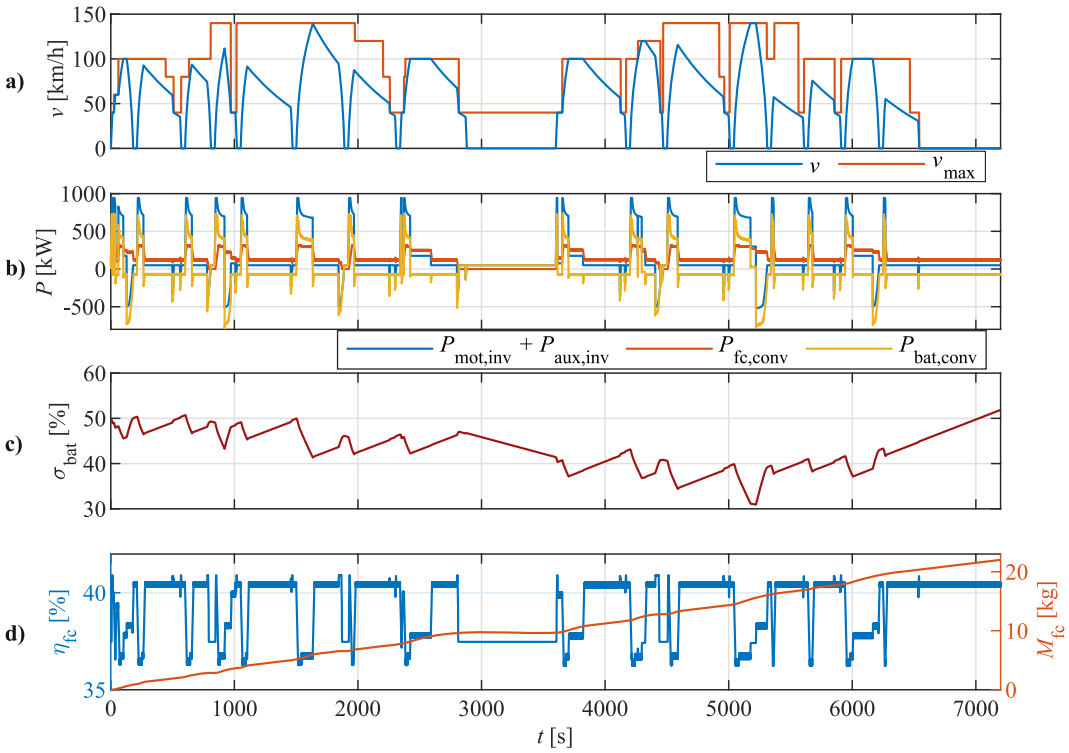

Fig. 8. Simulation results for the system operation in passenger train mode: (a) train velocity profile; (b) power profiles at the DC link; (c) battery state-of-charge; (d) efficiency of the fuel cell stack and cumulative consumption of hydrogen.

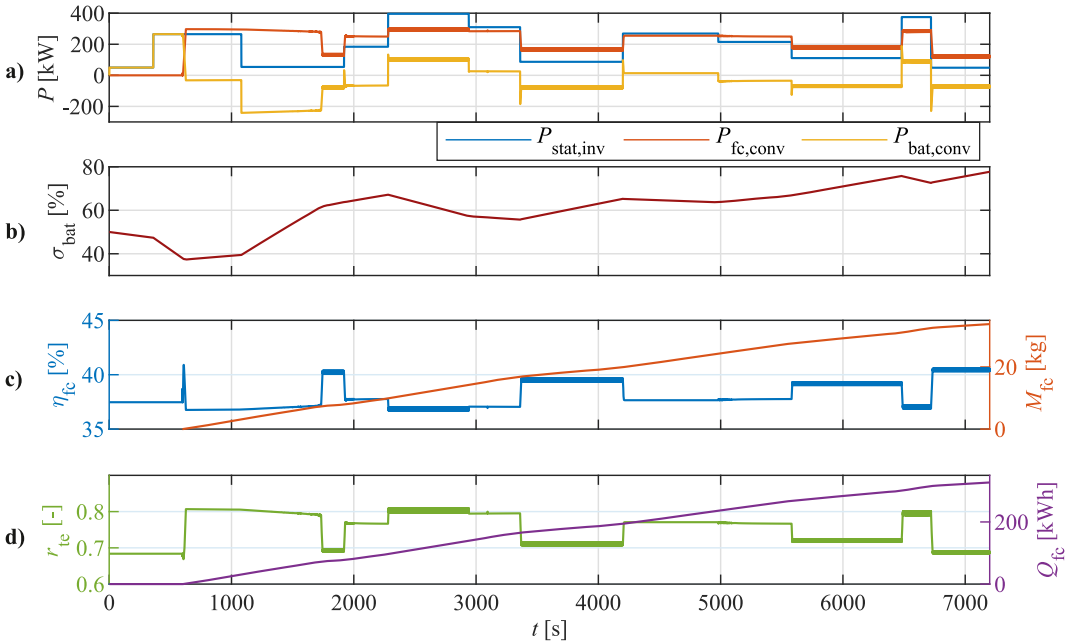

Fig. 9. Simulation results for the system operation in vehicle-to-grid mode: (a) power profiles at the DC link; (b) battery state-of-charge; (c) efficiency of the fuel cell stack and cumulative consumption of hydrogen; (d) thermal-to-electrical ratio and provided thermal energy from the fuel cell stack.

6. Conclusions

This paper presented the simulation-based assessment of hydrogen fuel cell hybrid-electric vehicle employed in a regular service as a regional passenger train, and as a cogenerative energy source in vehicle-to-grid (V2G) applications. The analysis included the development of a backward-looking quasi-static simulation model used for the evaluation of dynamics of individual system components, and the implementation of a real-time optimization-based energy management and control strategy for dispatching different power sources, namely, a fuel cell stack and a lithium-ion battery. The numerical experiments for selected benchmark vehicle and regional railway services in the Netherlands demonstrated the suitability of the proposed power control in ensuring proper system operation, while minimizing the overall hydrogen consumption. Obtained average hydrogen consumption for the 2-h vehicle round trip was 0.4 kg/km, with the overall electrical efficiency of 38.89%. The same vehicle satisfied complete stationary power demand in V2G scenario, and at the same time provided about 327 kWh of thermal energy, reaching overall cogeneration efficiency of 66.81%.

In summary, the innovative and high-performing V2G concept for hydrogen fuel cell hybrid-electric regional trains shows promising benefits for future smart grid applications. It offers numerous possibilities for future research, including system applications for other users such as residential buildings or low temperature district heating, as well as further studies related to the system integration into smart grids and/or real prototype developments. One of the main challenges is the development of an energy management strategy for the entire fleet during stabling periods, which would coordinate operation of different vehicles while maximizing energy efficiency of the whole system.

The current study considered a tank-to-wheel system performance. A wider-scope well-to-wheel approach will be required to account the energy losses from upstream processes linked to the hydrogen production and distribution (well-to-tank stage). As presented by JRC (2020), required well-to-tank energy per unit of the energy content of the final fuel for the electrolysis-produced hydrogen based on the EU electricity production mix for 2030 is more than three times higher than the wind power-based electrolysis scenario (2.72 MJ/MJ_{fuel} vs. 0.87 MJ/MJ_{fuel}), with associated greenhouse gasses more than twelve times higher (118.6 $kgCO_2e/MJ_{fuel}$ vs. 9.5 $kgCO_2e/MJ_{fuel}$). The well-to-wheel approach is crucial for a fair comparison with alternative systems and technical solutions that could be employed in similar contexts, such as battery-electric multiple units and/or opportunity charging by installing short catenary sections in selected stations. Such comparative analysis would contribute to the identification of optimal V2G deployment schemes of fuel cell vehicles.

Declaration of competing interest

The authors declare that they have no known competing financial interests or personal relationships that could have appeared to influence the work reported in this paper.

Acknowledgment

This work is supported by Arriva Personenvervoer Nederland B.V. within the PhD project “Improving sustainability of regional railway services” of Delft University of Technology.

References

Bagotsky, V.S., Skundin, A.M., Volfkovich, Y.M., 2015. Electrochemical power sources: batteries. In: Fuel Cells, and Supercapacitors. John Wiley & Sons,Inc., Hoboken, New Jersey.

Ballard, 2023. FCmove. Available online: https://www.ballard.com/about-ballard/publication_library/product-specification-sheets/fcmovetm-spec-sheet (Accessed on 29 April 2023).

Barbir, B., 2013. PEM Fuel Cells: Theory and Practice, second ed. Elsevier Inc. https://doi.org/10.1016/C2011-0-06706-6.

Bibak, B., Tekiner-Moğulkoç, H., 2021. A comprehensive analysis of Vehicle to Grid (V2G) systems and scholarly literature on the application of such systems. Renewable Energy Focus 36, 1–20. https://doi.org/10.1016/j.ref.2020.10.001.

Brünger, O., Dahlhaus, E., 2014. In: Hansen, I.A., Pachl, J. (Eds.), Running time estimation, Railway Timetabling & Operations. Eurailpress, Hamburg, pp. 65–89.

Calise, F., Cappiello, F.L., Dentice d'Accadia, M., Vicidomini, M., 2021. Smart grid energy district based on the integration of electric vehicles and combined heat and power generation. Energy Convers. Manag. 234, 113932 https://doi.org/10.1016/j.enconman.2021.113932.

Cao, S., 2016. Comparison of the energy and environmental impact by integrating a H 2 vehicle and an electric vehicle into a zero-energy building. Energy Convers. Manag. 123, 153–173. https://doi.org/10.1016/j.enconman.2016.06.033.

Davis, W.J., 1926. The tractive resistance of electric locomotives and cars. Gen. Electr. Rev. 29, 685–707.

Ercan, T., Noori, M., Zhao, Y., Tatari, O., 2016. On the front lines of a sustainable transportation fleet: applications of vehicle-to-grid technology for transit and school buses. Energies 9, 230. https://doi.org/10.3390/en9040230.

Fletcher, R., 2010. In: Di Pillo, G., Schoen, F. (Eds.), The sequential quadratic programming method, Nonlinear Optimization. Lecture Notes in Mathematics, vol. 1989. Springer, Berlin, pp. 165–214. https://doi.org/10.1007/978-3-642-11339-0_3.

Fragiacomo, P., Piraino, F., 2021. Vehicle-to-grid application with hydrogen-based tram. Energy Convers. Manag. 250, 114915 https://doi.org/10.1016/j.enconman.2021.114915.

Ghaviha, N., Campillo, J., Bohlin, M., Dahlquist, E., 2017. Review of application of energy storage devices in railway transportation. Energy Proc. 105, 4561–4568. https://doi.org/10.1016/j.egypro.2017.03.980.

Giro Batalla, R., Feenstra, M., 2012. Energy Consumption in GTW DMU Trains - ECO Driving. Project statement, Arriva Nederland.

Go, H.-S., Cho, I.-H., Kim, G.-D., Kim, C.-H., 2018. Reduction of electricity prices using the train to grid (T2G) system in urban railway. Energies 11, 501. https://doi.org/10.3390/en11030501.

Ham, S.-W., Jo, S.-Y., Dong, H.-W., Jeong, J.-W., 2015. A simplified PEM fuel cell model for building cogeneration applications. Energy Build. 107, 213–225. https://doi.org/10.1016/j.enbuild.2015.08.023.

Han, Y., Li, Q., Wang, T., Chen, W., Ma, L., 2018. Multisource coordination energy management strategy based on SOC consensus for a PEMFC–battery–supercapacitor hybrid tramway. IEEE Trans. Veh. Technol. 67, 296–305. https://doi.org/10.1109/TVT.2017.2747135.

Huerlimann, D., Nash, A., 2003. Opentrack-simulation of Railway Networks. User manual version 1.3.
İnci, M., Büyük, M., Savrun, M.M., Demir, M.H., 2021. Design and analysis of fuel cell vehicle-to-grid (FCV2G) system with high voltage conversion interface for sustainable energy production. Sustain. Cities Soc. 67, 102753 https://doi.org/10.1016/j.scs.2021.102753.
JRC, 2020. JEC Well-to-Tank report v5. In: Well-to-Wheels Analysis of Future Automotive Fuels and Powertrains in the European Context. Luxembourg. https://doi.org/10.2760/959137.
Kapetanović, M., Núñez, A., van Oort, N., Goverde, R.M.P., 2022. Analysis of hydrogen-powered propulsion system alternatives for diesel-electric regional trains. J. Rail Transp. Plann. Manag. 23, 100338 https://doi.org/10.1016/j.jrtpm.2022.100338.
Kapetanović, M., Núñez, A., van Oort, N., Goverde, R.M.P., 2021a. Reducing fuel consumption and related emissions through optimal sizing of energy storage systems for diesel-electric trains. Appl. Energy 294, 117018. https://doi.org/10.1016/j.apenergy.2021.117018.
Kapetanović, M., Vajihi, M., Goverde, R.M.P., 2021b. Analysis of hybrid and plug-in hybrid alternative propulsion systems for regional diesel-electric multiple unit trains. Energies 14, 5920. https://doi.org/10.3390/en14185920.
Klebsch, W., Guckes, N., Heininger, P., 2020. Evaluation of Climate-Neutral Alternatives to Diesel Multiple Units: Economic Viability Assessment Based on the Example of the ⟩Düren Network. VDE Report, Frankfurt am Main.
Leska, M., Aschemann, H., Melzer, M., Meinert, M., 2017. Comparative calculation of the fuel-optimal operating strategy for diesel hybrid railway vehicles. Int. J. Appl. Math. Comput. Sci. 27, 323–336. https://doi.org/10.1515/amcs-2017-0023.
Leska, M., Gruning, T., Aschemann, H., Rauh, A., 2013. Optimal trajectory planning for standard and hybrid railway vehicles with a hydro-mechanic transmission. In: 2013 European Control Conference (ECC), pp. 4550–4555. https://doi.org/10.23919/ecc.2013.6669576.
Li, H., Ravey, A., N'Diaye, A., Djerdir, A., 2019. Online adaptive equivalent consumption minimization strategy for fuel cell hybrid electric vehicle considering power sources degradation. Energy Convers. Manag. 192, 133–149. https://doi.org/10.1016/j.enconman.2019.03.090.
Luxfer, 2023. Specification Data: G-Stor H2 alternative fuel Cylinders. Available online: https://www.luxfercylinders.com/products/alternative-fuel/g-stor-h2-hydrogen-cylinders. (Accessed 19 April 2023).
Maleki, A., Rosen, M.A., 2017. Design of a cost-effective on-grid hybrid wind–hydrogen based CHP system using a modified heuristic approach. Int. J. Hydrogen Energy 42, 15973–15989. https://doi.org/10.1016/j.ijhydene.2017.01.169.
Miller, A., Erickson, T., Dippo, J., Eisele, R., Johnson, M., Lambrecht, T., 2011. Hydrogen fuel-cell locomotive: switching and power-to-grid demonstrations. In: Proceedings of World Congress on Railway Research.
Morais, H., Sousa, T., Vale, Z., Faria, P., 2014. Evaluation of the electric vehicle impact in the power demand curve in a smart grid environment. Energy Convers. Manag. 82, 268–282. https://doi.org/10.1016/j.enconman.2014.03.032.
Najafi, B., Haghighat Mamaghani, A., Baricci, A., Rinaldi, F., Casalegno, A., 2015. Mathematical modelling and parametric study on a 30 kWel high temperature PEM fuel cell based residential micro cogeneration plant. Int. J. Hydrogen Energy 40, 1569–1583. https://doi.org/10.1016/j.ijhydene.2014.11.093.
Oldenbroek, V., Hamoen, V., Alva, S., Robledo, C.B., Verhoef, L.A., van Wijk, A.J.M., 2018. Fuel cell electric vehicle-to-grid: experimental feasibility and operational performance as balancing power plant. Fuel Cell. 18, 649–662. https://doi.org/10.1002/fuce.201700192.
Oldenbroek, V., Smink, G., Salet, T., van Wijk, A.J.M., 2019. Fuel cell electric vehicle as a power plant: techno-economic scenario analysis of a renewable integrated transportation and energy system for smart cities in two climates. Appl. Sci. 10, 143. https://doi.org/10.3390/app10010143.
Oldenbroek, V., Wijtzes, S., van Wijk, A., Blok, K., 2017. Fuel cell electric vehicle to grid & H2: balancing national electricity, heating & transport systems a scenario analysis for Germany in the year 2050. In: 2017 IEEE Green Energy and Smart Systems Conference (IGESSC), pp. 1–6. https://doi.org/10.1109/IGESC.2017.8283458.
Özgirgin, E., Devrim, Y., Albostan, A., 2015. Modeling and simulation of a hybrid photovoltaic (PV) module-electrolyzer-PEM fuel cell system for micro-cogeneration applications. Int. J. Hydrogen Energy 40, 15336–15342. https://doi.org/10.1016/j.ijhydene.2015.06.122.
Paganelli, G., Delprat, S., Guerra, T.M., Rimaux, J., Santin, J.J., 2002. Equivalent Consumption Minimization Strategy for Parallel Hybrid Powertrains. IEEE 55th Vehicular Technology Conference, pp. 2076–2081. https://doi.org/10.1109/VTC.2002.1002989. VTC Spring 2002 (Cat. No.02CH37367).
Pesaran, A., Kim, G.-H., Gonder, J., 2005. PEM Fuel Cell Freeze and Rapid Startup Investigation. Milestone Report NREL/MP-540-38760. Golden, Colorado.
Pröhl, L., 2017a. OPEUS Deliverable DO2.1 - OPEUS Simulation Methodology. EU-project OPEUS (S2R-OC-CCA-02-2015).
Pröhl, L., 2017b. OPEUS Deliverable DO2.2 - OPEUS Simulation Tool. EU-project OPEUS (S2R-OC-CCA-02-2015).
Pröhl, L., Aschemann, H., 2019a. Energy optimal trajectory planning for electrically driven railway vehicles with particle swarm optimization. In: IEEE 15th International Conference on Control and Automation (ICCA), pp. 423–428. https://doi.org/10.1109/ICCA.2019.8900019.
Pröhl, L., Aschemann, H., 2019b. Grey wolf optimisation of an operating strategy for energy storage systems in electrically driven railway vehicles. In: 18th European Control Conference (ECC), pp. 1908–1913. https://doi.org/10.23919/ECC.2019.8795720.
Pröhl, L., Aschemann, H., Palacin, R., 2021. The influence of operating strategies regarding an energy optimized driving style for electrically driven railway vehicles. Energies 14 (3), 583. https://doi.org/10.3390/en14030583.
Qian, F., Gao, W., Yang, Y., Yu, D., 2020. Economic optimization and potential analysis of fuel cell vehicle-to-grid (FCV2G) system with large-scale buildings. Energy Convers. Manag. 205, 112463 https://doi.org/10.1016/j.enconman.2019.112463.
Robledo, C.B., Oldenbroek, V., Abbruzzese, F., van Wijk, A.J.M., 2018. Integrating a hydrogen fuel cell electric vehicle with vehicle-to-grid technology, photovoltaic power and a residential building. Appl. Energy 215, 615–629. https://doi.org/10.1016/j.apenergy.2018.02.038.
Sarma, U., Ganguly, S., 2018. Determination of the component sizing for the PEM fuel cell-battery hybrid energy system for locomotive application using particle swarm optimization. J. Energy Storage 19, 247–259. https://doi.org/10.1016/j.est.2018.08.008.
Stadler, 2005. GTW DMU-2 2/6 and GTW 2/8 Low-Floor for Arriva, Netherlands. Available online: https://www.stadlerrail.com/media/pdf/garr1008e.pdf (Accessed on 15 April 2023).
Sun, Y., Anwar, M., Hassan, N.M.S., Spiryagin, M., Cole, C., 2021. A review of hydrogen technologies and engineering solutions for railway vehicle design and operations. Railway Eng. Sci. 29, 212–232. https://doi.org/10.1007/s40534-021-00257-8.
Tao, S., Chen, W., Gan, R., Li, L., Zhang, G., Han, Y., Li, Q., 2021. Energy management strategy based on dynamic programming with durability extension for fuel cell hybrid tramway. Railway Eng. Sci. 29, 299–313. https://doi.org/10.1007/s40534-021-00247-w.
Torreglosa, J.P., Jurado, F., García, P., Fernández, L.M., 2011. Hybrid fuel cell and battery tramway control based on an equivalent consumption minimization strategy. Control Eng. Pract. 19, 1182–1194. https://doi.org/10.1016/j.conengprac.2011.06.008.
Toshiba, 2023. SCiB™ Rechargeable battery. Available online: http://www.global.toshiba/ww/products-solutions/battery/scib.html. (Accessed 14 April 2023).
Xu, L., Li, J., Ouyang, M., 2015. Energy flow modeling and real-time control design basing on mean values for maximizing driving mileage of a fuel cell bus. Int. J. Hydrogen Energy 40, 15052–15066. https://doi.org/10.1016/j.ijhydene.2015.08.104.
Zhang, W., Li, J., Xu, L., Ouyang, M., 2017. Optimization for a fuel cell/battery/capacity tram with equivalent consumption minimization strategy. Energy Convers. Manag. 134, 59–69. https://doi.org/10.1016/j.enconman.2016.11.007.
Zhuang, P., Liang, H., 2021. Stochastic energy management of electric bus charging stations with renewable energy integration and B2G capabilities. IEEE Trans. Sustain. Energy 12, 1206–1216. https://doi.org/10.1109/TSTE.2020.3039758.